J Stat Phys
DOI 10.1007/s10955-011-0320-x

Correlated Tunneling in Hydrogen Bonds

Lin Lin · Joseph A. Morrone · Roberto Car

Received: 9 June 2011 / Accepted: 12 August 2011

Abstract We study the quantum nature of the protons participating in hydrogen bonds in several ice structures by analyzing the one particle density matrix. We find that in all cases, including ice Ih, the most common form of ice, and the high pressure phases, ice VIII, VII, and X, the system is ground-state dominated. However, while the dynamics is uncorrelated in the structures with standard asymmetric hydrogen bonds, such as ice Ih and VIII, local correlations among the protons characterize ice VII and, to a lesser extent, ice X in the so-called low barrier hydrogen bond regime. The correlations appear along the path to hydrogen bond symmetrization, when quantum fluctuations delocalize the proton on the two bond sides. The correlations derive from a strong requirement for local charge neutrality that favors concerted motion along the bonds. The resulting behavior deviates substantially from mean field theory, which would predict in ice VII coherent tunneling of the proton between the two bond sides, thereby causing an ionization catastrophe. Due to the correlations, the quantum state of the proton is entangled.

Keywords Hydrogen bonding · Proton tunneling · High pressure ice phases

1 Introduction

It is well known that the dynamics of the protons participating in hydrogen (H) bonds is influenced by quantum mechanics even at room and at higher temperature. For instance,

L. Lin
Program in Applied and Computational Mathematics, Princeton University, Princeton, NJ 08544, USA

J.A. Morrone
Department of Chemistry, Princeton University, Princeton, NJ 08544, USA

Present address:
J.A. Morrone
Department of Chemistry, Columbia University, New York, NY 10027, USA

R. Car (✉)
Department of Chemistry and Physics, Princeton University, Princeton, NJ 08544, USA
e-mail: rcar@princeton.edu

Published online: 01 September 2011

deep inelastic neutron scattering (DINS) experiments show that the momentum distribution of the protons in condensed water phases differs significantly from the classical equilibrium distribution [1]. Moreover, diffraction experiments detect isotope effects upon deuterium for hydrogen substitution in the pair correlation functions of liquid water [2], and computational studies show that inclusion of nuclear quantum effects in *ab initio* molecular dynamics simulations of the liquid is needed to achieve quantitative agreement with the experimental structure [3]. Quantum effects are not limited to static properties but also influence the vibrational dynamics probed in inelastic neutron scattering [4] and infrared experiments [5–7]. In all these situations quantal behavior originates from zero-point motion. This effect is unusually large due to the small proton mass, yet it is quasi-harmonic and essentially semiclassical in nature [8, 9].

New physics occurs in presence of proton tunneling. This phenomenon plays an important role in phase transitions such as the ferroelectric to paraelectric transition in H-bonded KDP or the sequence of transitions leading to H bond symmetrization in pressurized ice. These transitions exhibit large isotope effects that can only be explained by invoking quantum fluctuations. Here we focus in particular on ice VIII, VII and X as these phases epitomize the H bond symmetrization transformation that takes place when the oxygen-oxygen nearest neighbor separation is progressively reduced by applying pressure, thereby mutating the ice crystal from an H-bonded molecular system to a heteroatomic system with covalent/ionic bonds. The lower pressure phase ice VIII is characterized by the usual asymmetric H bonds, similar to those found in ice Ih, the stable ice structure at standard temperature and pressure. In these phases each molecule is bonded to four neighboring molecules and the proton distribution in the lattice of H bonds satisfies the ice rules [10, 11]. A configuration satisfies the ice rules if on the four bonds connecting an oxygen to its neighbors two hydrogens (protons) are near the central oxygen and two are near the neighboring oxygens, as is required to keep the water molecules intact. While disordered in ice Ih, the proton lattice is ordered in ice VIII engendering an antiferroelectric arrangement of molecular dipoles. Long range antiferroelectric order is lost in the phase occurring at intermediate pressure, ice VII, where the protons can be found with equal probability on the two bond sites. The transition from ice VIII to ice VII can be viewed as an order-disorder transition leading from an antiferroelectric to a paraelectric crystal. Lastly, in ice X, which is the phase at the highest pressure, H bond symmetrization is complete and the probability distribution of the proton along the bond is unimodal and centered at midbond.

The important role of quantum tunneling in the transformation from ice VIII to VII was first suggested by Stillinger and Schweizer in a series of remarkable papers based on an insightful but simplified model for the proton sublattice. In the first of these papers [12] the authors adopted a mean field approximation describing the transition in terms of independent protons tunneling coherently back and forth between the two off-center bond sites. In the subsequent papers [13, 14] they pointed out that, although qualitatively correct, the mean field description was not to be trusted quantitatively as it led to a complete ionization catastrophe accompanied by a large deviation of the ice rules. Correlations among the protons should oppose coherent tunneling, they noticed, in order to partially restore the ice rules and the charge neutrality of the water molecules. The crucial role of tunneling in the H bond symmetrization transitions was confirmed 15 years later in a cutting-edge *ab initio* simulation by Parrinello and collaborators [15]. This study adopted Feynman's path integral formulation of quantum statistical mechanics to sample the equilibrium configurations of the oxygen and hydrogen nuclei in a periodically repeated supercell containing 16 water molecules. In this approach the nuclei can take any position in space (an off-lattice model) and are treated quantum mechanically without recourse to mean field or variational approximations as in Refs. [12–14]. Thermal effects are also included while Refs. [12–14] were

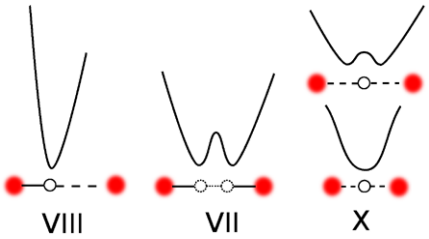

Fig. 1 (Color online) Cartoon depicting the understanding established in the literature. As pressure is increased the bond undergoes a transition from single welled (ice VIII) to a high-barrier (HBHB, ice VII) and then low-barrier (LBHB, ice X) double welled potentials until a unimodal form centered at the midpoint (highest pressure, ice X) persists

limited to $T = 0$ K. Finally, in Ref. [15] the internuclear interactions were generated from first-principles, *i.e.* they were obtained on the fly from the instantaneous ground state energy of the electrons, calculated accurately, albeit approximately, within electronic density functional theory (DFT). This approach avoids empirical parameterization of the interatomic force field, an important aspect in the context of the H bond symmetrization transformation in which the character of the interatomic bonds, the electron charge distribution, and the potential experienced by the protons are all expected to undergo considerable changes. Besides confirming that proton tunneling drives the transitions Ref. [15] reported a novel prediction, namely that zero point motion leads to H bond symmetrization before the potential experienced by the proton converts from a double to a single well. This finding suggested the following classification of H bonds: (i) at large inter-oxygen separations such as $d_{\mathrm{OO}} \sim 2.78$ Å, typical of ice Ih, or $d_{\mathrm{OO}} \sim 2.53$ Å, typical of ice VIII, standard H bonds are present in which the tunnel splitting is zero or negligibly small and the protons experience an effective asymmetric single well potential, (ii) at intermediate separations such as $d_{\mathrm{OO}} \sim 2.45$ Å, typical of ice VII, so called high barrier H bonds (HBHB) are present in which tunnel splitting is non-negligible and larger than the thermal energy, and at least one of the split levels falls well below the top of the barrier between the two wells along a bond so that quantum tunneling originates a bimodal proton distribution, (iii) at shorter separations such as $d_{\mathrm{OO}} \sim 2.31$ Å within the stability range of ice X, so-called low barrier H bonds (LBHB) are present in which the potential remains double welled but the proton distribution is unimodal due to zero-point motion, (iv) at even shorter separations within the stability range of ice X, the potential becomes single welled as illustrated in Fig. 1.

The picture in Fig. 1 is suggestive but still rooted in mean field theory. Even though the path integral simulation included proton correlations consistent with the finite size of the periodic supercell and with the adopted DFT approximation for the Born-Oppenheimer potential energy surface, Ref. [15] did not consider the role of correlations in forming its picture. These could only be monitored to limited extent in a simulation that only accessed the particle density in space. The proton density distribution, $n(\mathbf{r})$, is the diagonal part of the corresponding single particle density matrix $\rho(\mathbf{r}, \mathbf{r}')$. Access to diagonal and off-diagonal components of $\rho(\mathbf{r}, \mathbf{r}')$ provide more direct information about correlations. Indeed, for a system in the ground state the density matrix is idempotent, *i.e.* $\rho^2 = \rho$, when correlations are absent, while deviations from idempotency, signal entanglement due to correlations. Recently, we performed *ab initio* path integral simulations of ice Ih [3], VIII, VII, and X [16], in which we employed the same methodology of Ref. [15] but sampled open in addition to closed Feynman paths, thus allowing access to the full single-particle density matrix $\rho(\mathbf{r}, \mathbf{r}')$ of the protons. The so called end-to-end distribution of the Feynman paths $\widetilde{n}(\mathbf{x})$ is defined

as $\int \mathrm{d}\mathbf{r}\,\mathrm{d}\mathbf{r}'\,\rho(\mathbf{r},\mathbf{r}')\delta(\mathbf{r}-\mathbf{r}'-\mathbf{x})$: it is the distribution of the distances separating the two opposite ends of an open Feynman path. The Fourier transform of $\widetilde{n}(\mathbf{x})$ yields the momentum distribution $n(\mathbf{p})$ of a quantum particle. In the case of the protons this quantity can be directly compared to available DINS experiments. The proton momentum distribution was calculated in this way in Ref. [3] for liquid water and ice Ih, and in Ref. [16] for ice VIII, VII and X. Correlations among the protons, not considered in the cited publications, are the subject of this paper. We limit the discussion to ice. We start by demonstrating that the basic physics can be unveiled by considering a reduced model in which only the projection of the density matrix along a bond, $\rho(x,x')$, is taken into account. This follows from statistical analysis showing that proton motions along the bond are uncorrelated from the perpendicular motions, and is consistent with simple intuition suggesting that correlations should play a role only when the displacements along the bond are so large as to break the ice rules.

In both ice Ih at $T = 269$ K and in ice VIII at $T = 100$ K $\rho(x,x')$ is idempotent within the statistical errors of the simulation, indicating that the proton is approximately in a pure quantum state. Finding that these systems are ground state dominated is not surprising as stretching motions in common H bonds have frequencies around 3000 cm^{-1} and the zero point energy is much larger than $k_B T$. Interestingly, in ice VII at $T = 100$ K, a system with HBHB, large deviations from idempotency are found. Deviations from idempotency reduce significantly but are still visible in ice X at $T = 100$ K, when LBHB are present. The mixed state character of the density matrix $\rho(x,x')$ may be due to thermal and/or correlation effects, but our analysis shows that the latter dominate. Collective tunneling is a consequence of the ice rules that act to protect the integrity of the water molecules and reduce the likelihood of ionized configurations such as H_3O^+ and OH^-. In ice VII correlations favor concerted tunneling of the protons. Interestingly, correlation effects can also be detected in ice X when LBHB are present and individual water molecules can no longer be identified as the proton density distribution on the bond has become symmetric and unimodal. In this case correlations manifest as charge density waves that reflect dipolar fluctuations on the bonds. In both cases, that of HBHB and that of LBHB, the requirement of local charge neutrality is the mechanism that constrains quantum fluctuations causing correlated dynamics.

Plots like the one in Fig. 1 are very useful to illustrate the H bond symmetrization transformation but are an oversimplification. To make the picture more quantitative it is convenient to construct the effective potential that simultaneously fits $n(x)$ and $\widetilde{n}(x)$, *i.e.* the positions and the end-to-end distribution of the proton along the bond. In ice Ih and VIII, which are effectively in a pure quantum state at the temperature of the simulation, position and end-to-end distributions convey the same information. In fact both distributions are simply expressed in terms of the real ground state wavefunction $\psi(x)$ of the proton along the bond: $n(x) = \psi(x)^2$ and $\widetilde{n}(x) = \int \mathrm{d}y\,\psi(y+x)\psi(y)$. The effective bond potential for the proton provides a unique perspective on the anharmonicity of the proton environment. Anharmonicity is substantially larger in ice VIII than in ice Ih, as one would expect for a system close to the onset of tunneling fluctuations. In the presence of tunneling we are unable to find a unique potential that simultaneously fits the position and end-to-end distributions. This signals that the proton is no longer in a pure state but is in an entangled state due to its correlations with the other protons. When this occurs the proton can only be described by a potential ensemble reflecting its mixed quantum state character. This analysis leads to a new picture of the H bond symmetrization transformation that is presented in this paper.

It has been pointed out that proton dynamics hindered by ice rule correlations has similarities with the physics of strongly correlated electron systems near the Mott-Hubbard transition [17]. The analogy is even closer with frustrated magnetic systems, that precisely for that reason have been dubbed spin ices, *i.e.* materials in which spin fluctuations are

hindered by constraints equivalent to the ice rules [18]. Correlations in these systems are usually investigated within coarse grained models that deal with a restricted set of dynamical variables and typically neglect coupling to the lattice. We use instead a realistic model that includes all the degrees of freedom and treats thermal and quantum fluctuations on equal footing. As a downside we face severe limitations on the size of the simulation cell and could only perform few simulations at different lattice parameters. In spite of these limitations some general qualitative effects emerged from the simulations: (i) correlations are important whenever tunneling occurs; (ii) concerted ring tunneling, *i.e.* the only process allowed by ice rules, does occur but less frequently than less extended collective motions indicating some violation of the ice rules; (iii) fleeting ionized configurations do occur but with substantially less charge separation frequency than the mean field prediction.

The paper is organized as follows. In Sect. 2 we give the path integral representation of the single particle density matrix with details of the simulations, and discuss the evidence supporting separability of the equilibrium dynamics along the bond from that in the plane perpendicular to the bond. The resulting bond model is discussed in Sect. 3 where we report a singular value decomposition of the density matrix $\rho(x, x')$, yielding occupation numbers and eigenstates. Pure and mixed states of the proton are discussed in this context, and an analysis is presented to show that thermal effects are negligible compared to correlation effects in both HBHB and LBHB cases. In Sect. 4 the correlations are discussed with reference to local charge neutrality and population of ionized defects, for which simulation results and mean field values are compared. We also discuss in this section the statistics of the fluctuating H bond patterns along closed hexagonal rings in the ice VII simulation, showing substantial deviation from the mean field picture. In Sect. 5 we discuss how space and end-to-end distributions can be mimicked by an ensemble of effective bond potentials for the proton. This analysis leads to a new picture of the sequence of H bond symmetrization transitions. Finally, in Sect. 6 we conclude with general considerations and comment on the consequences of the present findings in the more general context H-bonded systems.

2 Reduced Longitudinal Model

In what follows we indicate by $\mathbf{r}_i$ the spatial coordinates of particle (proton or oxygen nucleus) i ($i = 1, \ldots, M$). The single particle density matrix for the i-th particle is given by

$$\rho_i(\mathbf{r}, \mathbf{r}') = \frac{1}{Z} \int \mathrm{d}\mathbf{r}_1 \cdots \mathrm{d}\mathbf{r}_{i-1}\, \mathrm{d}\mathbf{r}_{i+1} \cdots \mathrm{d}\mathbf{r}_M \langle \mathbf{R} | e^{-\beta \hat{H}} | \mathbf{R}' \rangle. \tag{1}$$

Here β is the inverse temperature and $\mathbf{R}$ and $\mathbf{R}'$ indicate the collection of spatial coordinates

$$\mathbf{R} = \big(\mathbf{r}_1, \ldots, \mathbf{r}_{i-1}, \mathbf{r}, \mathbf{r}_{i+1}, \ldots, \mathbf{r}_M\big),$$
$$\mathbf{R}' = \big(\mathbf{r}_1, \ldots, \mathbf{r}_{i-1}, \mathbf{r}', \mathbf{r}_{i+1}, \ldots, \mathbf{r}_M\big).$$

The many body Hamiltonian operator $\hat{H}$ for the nuclei includes the kinetic energy and the many body potential energy surface $V(\mathbf{r}_1, \ldots, \mathbf{r}_M)$,

$$\hat{H} = \sum_{i=1}^{M} \frac{\mathbf{p}_i^2}{2m_i} + V(\mathbf{r}_1, \cdots, \mathbf{r}_M). \tag{2}$$

Z, the partition function of the system, is defined by

$$Z = \mathrm{Tr}\left[e^{-\beta \hat{H}}\right]. \tag{3}$$

Protons are associated to H bonds connecting two neighboring oxygens. We denote by x_i the position of proton i along the H bond to which it belongs. x_i is the longitudinal component of $\mathbf{r}_i$ and $\mathbf{b}_i$ is the corresponding transverse component, *i.e.* $\mathbf{r}_i = (x_i, \mathbf{b}_i)$. The longitudinal density matrix for particle i, $\rho_i(x, x')$, is the corresponding single particle density matrix projected along the bond

$$\rho_i(x, x') = \int \mathrm{d}\mathbf{b}\, \mathrm{d}\mathbf{b}' \rho_i(\mathbf{r}, \mathbf{r}'). \tag{4}$$

In all the systems that we will discuss below, the protons are embedded in the crystal environment and can be assumed to be equivalent except for the differences in their orientation. The longitudinal density matrix further eliminates the difference in orientation, as all the longitudinal density matrices are essentially the same in the local bond frame. In what follows we drop the subscript i and simply indicate the longitudinal density matrix by $\rho(x, x')$.

Two physical properties extracted from the reduced density matrix $\rho(x, x')$ will be used extensively throughout this paper. One is the position distribution of a proton, given by:

$$n(x) = \int \mathrm{d}y\, \delta(y - x)\rho(y, y). \tag{5}$$

The other is the so-called end-to-end distribution, given by:

$$\widetilde{n}(x) = \int \mathrm{d}y\, \mathrm{d}y'\, \delta(y - y' - x)\rho(y, y'). \tag{6}$$

The Fourier transform of the end-to-end distribution gives the momentum distribution.

For distinguishable quantum particles,[1] the density matrix $\rho_i(\mathbf{r}, \mathbf{r}')$, and therefore the longitudinal density matrix $\rho(x, x')$, can be represented using the imaginary time path integral formalism [19]

$$\rho_i(\mathbf{r}, \mathbf{r}') = \frac{1}{Z} \int_{\mathbf{R}(0)=\mathbf{R}, \mathbf{R}(\beta\hbar)=\mathbf{R}'} \mathfrak{D}\mathbf{R}(\tau) e^{-\frac{1}{\hbar}\int_0^{\beta\hbar} d\tau \frac{m\dot{\mathbf{R}}^2(\tau)}{2} + V(\mathbf{R}(\tau))}. \tag{7}$$

The partition function Z takes the form

$$Z = \int_{\mathbf{R}(0)=\mathbf{R}, \mathbf{R}(\beta\hbar)=\mathbf{R}} \mathfrak{D}\mathbf{R}(\tau) e^{-\frac{1}{\hbar}\int_0^{\beta\hbar} d\tau \frac{m\dot{\mathbf{R}}^2(\tau)}{2} + V(\mathbf{R}(\tau))}. \tag{8}$$

The compact notation $\mathbf{R}(\tau)$ is used here to represent a path of all M particles along the imaginary time axis

$$\mathbf{R}(\tau) = \big(\mathbf{r}_1(\tau), \ldots, \mathbf{r}_{i-1}(\tau), \mathbf{r}_i(\tau), \mathbf{r}_{i+1}(\tau), \ldots, \mathbf{r}_M(\tau)\big). \tag{9}$$

In (7) a path starts at $\mathbf{R}$ and ends at $\mathbf{R}'$, whereas in (8) a path starts and ends at the same point $\mathbf{R}$. $V(\mathbf{R}(\tau))$ is the many body potential evaluated on the imaginary time slice τ *i.e.*

[1] Identical particles such as protons are distinguishable when exchange processes can be neglected.

$V(\mathbf{r}_1(\tau), \ldots, \mathbf{r}_M(\tau))$. The partition function Z (8) involves closed Feynman paths for all the particles, whereas in the density matrix (7) the path corresponding to particle i is open and the paths of all the other particles are closed. In numerical implementations the action integrals in (7) and (8) are discretized by dividing the imaginary time interval of length $\hbar\beta$ into small time segments $\Delta\tau = \frac{\hbar\beta}{P}$. The integer P is the number of beads or system replicas. At finite temperature $T = \beta^{-1}$ the discretization error can be made as small as necessary by using an appropriate number of beads. The multidimensional integrals in (7) and (8) take the form of classical statistical integrals for the configurations of a set of polymer chains having P beads each. Thus, by adopting a discrete path integral representation quantum statistical mechanics is mapped exactly, within numerical accuracy, onto classical statistical mechanics. This so-called quantum-classical isomorphism [20] is very important as it allows us to compute equilibrium statistical properties of a quantum many-body system in terms of statistical averages of a corresponding effective classical system. The latter can be computed using numerical methods such as Monte Carlo and molecular dynamics.

The potential energy $V(\mathbf{r}_1, \mathbf{r}_2, \ldots, \mathbf{r}_M)$ in the Hamiltonian $\hat{H}$ defines the physical system of interest. In the present study $V(\mathbf{R}(\tau))$ is computed, according to the Born-Oppenheimer approximation, from the ground-state energy of the electrons with the nuclei in the configuration $\mathbf{R}(\tau)$. The electronic ground-state is solved within density functional theory [21, 22]. In the discretized path integral context, the Kohn-Sham electron orbitals [22] ϕ_i need to be calculated independently at all P imaginary time slices. In our simulation the statistically important polymer chain configurations $\mathbf{R}(\tau)$ are explored by molecular dynamics using forces generated on the fly according to the Car-Parrinello prescription [23] from the electronic ground states at P imaginary time slices. This procedure is called path integral Car-Parrinello molecular dynamics (PICPMD) or path integral *ab initio* molecular dynamics [24–26]. The advantage of this approach is that it avoids empirical parameterizations of the interatomic force field, contrary to commonly made approximations in most molecular dynamics and Monte Carlo simulations of multi-atomic systems. The *ab initio* approach is computationally more expensive than empirical force fields, but is also more accurate and has substantially improved predictive power. This is important in the present context as the interatomic bonds, the electronic charge distribution, and the potential experienced by the protons all undergo considerable changes during the H bond symmetrization transformations. In ice VII, in particular, bond forming and breaking events take place frequently in connection with proton tunneling.

PICPMD simulations sampling closed and open Feynman paths have been recently reported for a variety of water phases, liquid and crystalline [3, 15, 16, 27, 28]. Here we focus on the crystalline data and refer to Refs. [3] and [16] for the technical details of the simulations. We consider the common form of ice at standard pressure, ice Ih, and the high pressure phases ice VIII, ice VII, and ice X. In familiar phases such as hexagonal (Ih) ice and liquid water the proton is localized in a potential well asymmetrically placed on the bond between two neighboring oxygens. Thus there is a clear distinction between the polar covalent bond of the proton with the closer oxygen and the H bond with the more distant oxygen. In the high pressure phase ice VIII, the oxygen-oxygen (OO) distance is shortened, thereby increasing the anharmonicity of the covalent bond. At shorter OO distances, in ice VII, the proton acquires a bimodal distribution with maxima on the two sides of the OO bond. At sufficiently low temperatures the transition from the anti-ferroelectrically ordered arrangement of the protons in ice VIII to the proton disordered arrangement in ice VII is driven by quantum tunneling. At still shorter OO distances, a new phase is formed, ice X, in which the proton distribution is unimodal and centered at midbond: this configuration is often referred to as symmetric H bond. Typical OO distances for the four phases considered in

Table 1 The average distance ($\bar{x}$) between the proton and the nearest oxygen projected along the OO direction, and the distance between the two nearest oxygens (d_{OO}) in the structures used in this paper for ice Ih, VIII, VII and X

Phase	$\bar{x}$ (Å)	d_{OO} (Å)
Ih	0.993	2.78
VIII	1.014	2.53
VII	1.234	2.45
X	1.148	2.31

Table 2 Spearman's rank correlation coefficient for the end-to-end vector distance along and orthogonal to the hydrogen bonding direction in ice Ih, VIII, VII and X

System	R
Ih	0.029
VIII	0.032
VII	0.027
X	0.025

this paper are given in Table 1. The path integral data of Refs. [3] and [16] give access to the one particle density matrix $\rho(\mathbf{r}, \mathbf{r}')$ of the proton, or, equivalently, its position and end-to-end distributions. Here we use these data to study effects that were not discussed previously, namely how the correlations among the protons are affected by a changing environment.

Our study is greatly facilitated by the fact that, within the statistical accuracy of the data, the density matrix factorizes into a longitudinal and a transverse component relative to the bond, *i.e.* $\rho(\mathbf{r}, \mathbf{r}') \sim \rho(x, x')\rho(\mathbf{b}, \mathbf{b}')$. In other words position and end-to-end distributions along the bonding direction and in the plane orthogonal to it are mutually independent. The separation between bonding and transverse directions is valid in the sense of Spearman's rank correlation coefficient R (see the Appendix for the test of independence between two random variables using Spearman's rank correlation coefficient). The Spearman's R calculated for the end-to-end distances along and orthogonal to the hydrogen bonding direction in Ice Ih, VIII, VII and X is listed in Table 2. The Spearman's R is universally small across the different ice phases, strongly supporting factorization of the density matrix. In the case of ice Ih, factorization could be expected because in a recent work we have shown that the momentum distribution has an effective quasi-harmonic (Gaussian) form with 3 principal frequencies associated to longitudinal and transverse motions, respectively, relative to the bond [9]. The three high pressure phases considered here are characterized by much stronger anharmonicity along the bonding direction, well beyond the quasi-harmonic model. It is interesting that even in these cases quantitative analysis shows that longitudinal-transverse decoupling holds. It means that anharmonicity remains confined in the longitudinal direction in accord with simple chemical intuition.

3 Longitudinal Density Matrix

Let $\rho(x, x') = \langle x|\rho|x'\rangle$ be the normalized longitudinal density matrix, *i.e.* $\mathrm{Tr}[\rho] = 1$. If $P(i)$ denotes the eigenvalues of ρ and $|\phi(i)\rangle$ are the corresponding eigenvectors, one has:

$$\rho = \sum_i |\phi(i)\rangle P(i) \langle\phi(i)|. \tag{10}$$

Here $P(i)$ is the equilibrium population (occupation probability) of the state $|\phi(i)\rangle$ and $\sum_i P(i) = 1$. The spectrum of the density matrix is very instructive. If only one eigenvalue,

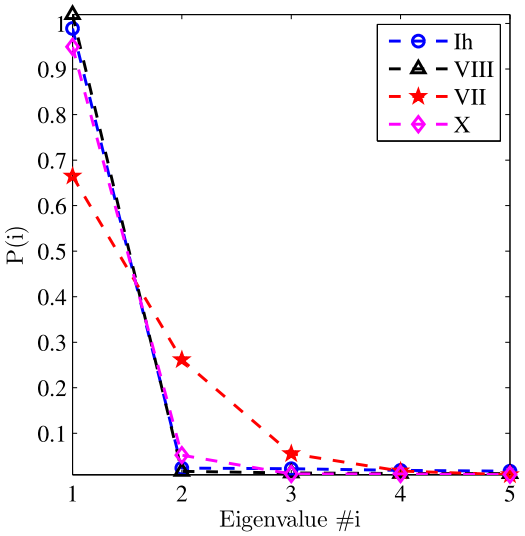

Fig. 2 (Color online) The first 5 eigenvalues of the longitudinal density matrix for ice Ih, VIII, VII and X. Within the accuracy of the simulation, $P(1) = 1$ for ice Ih and ice VIII, $P(1)$, $P(2)$, and $P(3)$ are different from zero for ice VII, $P(1)$ and $P(2)$ are different from zero for ice X. The ice Ih trajectory is shorter and the corresponding eigenvalues are affected by larger error bars than the three high pressure phases

$P(1)$, is different from zero, the density matrix is idempotent *i.e.* $\rho^2 = \rho$ and the equilibrium ensemble of the proton along the bond is pure, corresponding to the quantum state $|\phi(1)\rangle$. If more than one eigenvalue is different from zero, the density matrix deviates from idempotency, *i.e.* $\rho^2 < \rho$ and the equilibrium ensemble of the proton is mixed.

We bin the PICPMD simulation data [16] for the longitudinal density matrix with a spacing $\Delta x = 0.015$ Å and the corresponding discretized density matrix is diagonalized. The largest 5 eigenvalues of the longitudinal density matrix in ice Ih, VIII, VII and X are reported in Fig. 2. We find that both ice Ih at $T = 269$ K and ice VIII at $T = 100$ K have idempotent density matrix within the statistical errors of the simulation, indicating that the proton is in a pure quantum state. Thus, in these ices the proton motions along the bond are on average uncorrelated and the systems are ground state dominated at their respective temperatures. This is not surprising as the stretching motions in standard H bonds have typical frequencies around 3000 cm^{-1} corresponding to a zero point energy much larger than $k_B T$. Interestingly, in the case of ice VII at $T = 100$ K, which is in the HBHB regime, we find large deviations from idempotency. Deviations from idempotency are significantly reduced but still visible in ice X, which is in the LBHB regime. Deviation from idempotency indicates ice VII and X are not in a pure but in a mixed quantum state. Mixed state character of the longitudinal density matrix $\rho(x, x')$ may result from thermal or correlation effects or from a combination of both. Our analysis shows that correlations dominate in both ices at $T = 100$ K.

To infer the relative importance of thermal and correlation effects we adopt a two state model. This is a good approximation given the small value of the third eigenvalue, which is nonzero only in ice VII. In this ice we take $P(1) = 0.72$ and $P(2) = 0.28$ by renormalizing to 1 the sum of the first two eigenvalues in Fig. 2. We then consider an effective single particle 1D Hamiltonian that includes a kinetic energy term (with the proton mass) and a quartic double well potential term. We optimize the potential so that the 1D Hamiltonian has the two populated eigenvectors of the reduced density matrix as its two lowest energy states. The optimal potential is depicted in Fig. 3 and is given by

$$V(x) = 0.1100x^4 - 0.0475x^2 + 0.0051, \tag{11}$$

where we added a constant term to shift the minimum of the potential wells to 0.

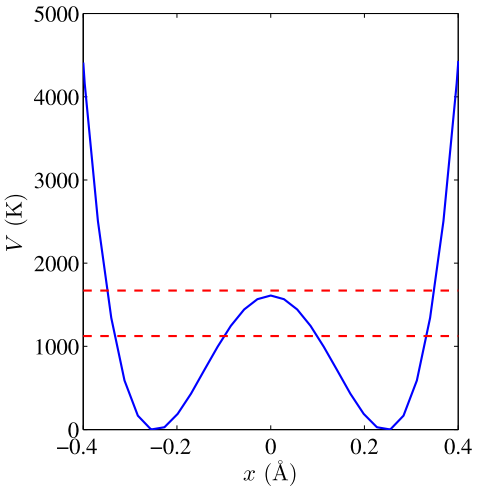

Fig. 3 (Color online) The optimized quartic double well potential that reproduces the lowest two states of the longitudinal density matrix. The *horizontal dashed lines* indicate the ground and the first excited state of this potential, respectively

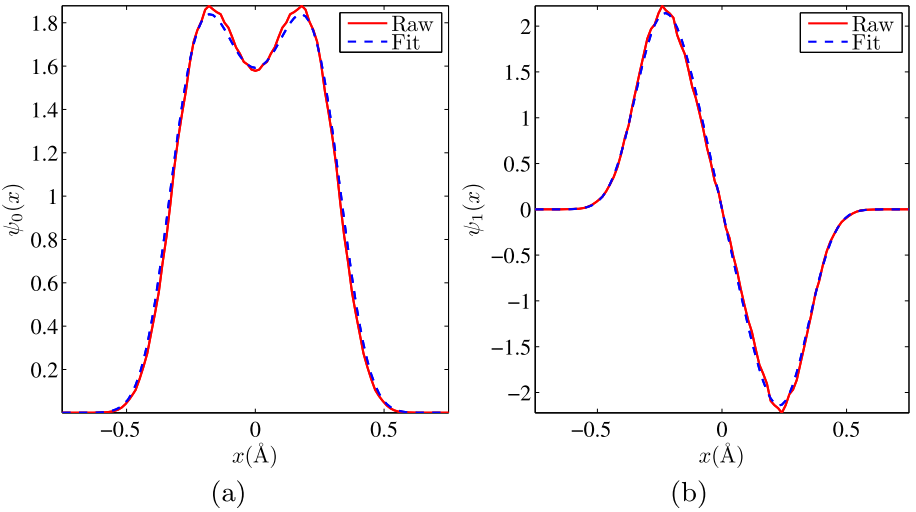

Fig. 4 (Color online) (**a**) The largest singular vector of the longitudinal density matrix (*red solid line*) and the ground state of the quartic potential in (11) (*blue dashed line*). (**b**) The second largest singular vector of the longitudinal density matrix (*red solid line*) and the first excited state of the quartic potential in (11) (*blue dashed line*)

Figure 4 compares the eigenvectors of the density matrix (labeled "Raw") and the eigenvectors of the quartic potential with optimal parameters (labeled "Fit"). The first two singular vectors of the density matrix are indeed very well approximated by the optimal potential.

The energies of the two lowest eigenvalues of the 1D Hamiltonian are given in Fig. 3. The corresponding tunnel splitting, 547 K, is much larger than the equilibrium temperature of the simulation (100 K), indicating that thermal effects are not the major cause of the mixed

character of the equilibrium proton ensemble.[2] Notice that the barrier height (1614 K) is well above the ground state energy (1124 K), confirming the HBHB character of ice VII. The analysis does not change appreciably if we include the third populated eigenstate of the density matrix: in that case the same procedure gives a tunnel splitting of 548 K. The potential in Fig. 3 can be viewed as a mean field potential for the proton: it is qualitatively (and even quantitatively) very similar to the mean field potential that was suggested for a tunneling proton in Ref. [12] on the basis of phenomenological considerations. In the mean field approximation each proton moves in a self-consistent potential that includes the effect of the other protons in an average way. The fact that a system which is ground state dominated is not in the ground state of the mean field potential indicates that correlations, neglected in the mean field approximation, are important. These correlations reflect the ice rules that act to retain the integrity of the water molecules, *i.e.* the local charge neutrality, when the protons tunnel between the two sides of a bond.

The pure versus mixed state character of the equilibrium ensemble is well characterized in terms of the entanglement (or von Neumann) entropy. This is defined as $S = -\mathrm{Tr}[\rho \log \rho]$. Using the eigenvalues reported in Fig. 2 we find that S is essentially 0 in ice Ih and VIII, indicating pure state character. On the other hand, $S = 0.60$ in ice VII and $S = 0.20$ in ice X, indicating mixed state character in both cases but with a larger entanglement in ice VII than in ice X.

4 Proton Correlations

Proton correlations originate from the requirement of local charge neutrality that favors intact water molecules over ionized configurations such as H_3O^+ and OH^-. These effects can be quantified by monitoring the deviation from local charge neutrality at each oxygen site in terms of the centroids of the Feynman paths for the protons. According to the position of the centroid along a bond we may assign the corresponding proton to either one of the two oxygens linked by the bond. We call the two corresponding proton sites N (near) and F (far), respectively, relative to one of the oxygens. Local charge neutrality demands that each oxygen has two N and two F protons on the four bonds with the neighboring oxygens: this is called the ice rule [10, 11]. In our simulation the rule is obeyed with probability $P = 1$ in ice VIII and ice Ih, but we find $P = 0.85$ in ice VII. This is to be compared with the mean field value $P_{MFA} = 0.375$ [12] in which protons randomly occupy the two sites. The large discrepancy between simulation and mean field theory, underlines the important role of correlations which oppose the formation of ionized species. The above discussion corresponds to a two-state model for the proton. We find, however, that a three-state model, in which the proton can occupy three distinct sites, N, F, and C (center) represents the simulation data more accurately. A path with a centroid near the bond center (C) is delocalized on the bond and the corresponding proton can be assigned with equal weight ($1/2$) to two oxygens. The boundaries of the respective states are defined according to regions of the centroid distribution projected along the bond. Although the precise definition of the boundaries is not unique the physics is consistent for reasonable choices. In this model local charge neutrality is satisfied not only by configurations like *NNFF* but also by configurations such as *NFCC* and *CCCC*, which would violate the strict ice rule. In the simulation we find that C states

[2] This result is entirely consistent with a previous study [16] that position and end-to-end distributions of the proton in ice VII could be modeled by an effective potential only by invoking a temperature significantly higher than the temperature of the simulation.

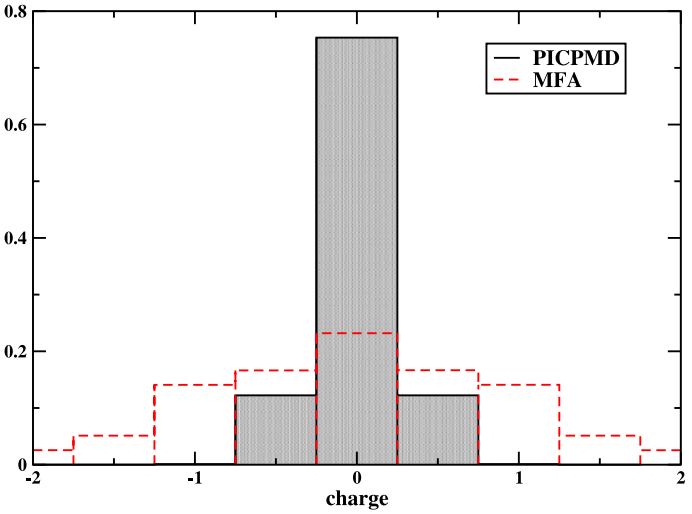

Fig. 5 (Color online) The distribution of local charge density in Ice VII according to the 3-state model discussed in the text (*gray bars*). This result can be seen to be in stark contrast to the randomly distributed set of charged species predicted by the mean field approximation (*dashed, red bars*)

occur with approximately half the frequency of either N or F states. Local change neutrality is satisfied with $P = 0.75$ as compared with a mean field value $P_{MFA} = 0.23$, indicating that the fractional deviation of the simulation from mean field is larger in the three-state than in the two-state model. Furthermore, the distribution of charged species is far narrower in our results as is illustrated in Fig. 5. In particular we find that in $> 99\%$ of species that violate charge neutrality there is a net charge of only ± 0.5, indicating that fully ionized species such as H_3O^+ are exceedingly rare.

One mechanism for proton tunneling is the creation of short-lived ionic configurations. This is in contrast to concerted proton tunneling along the closed water rings that comprise the crystal structure. In our simulation ice VIII and VII have BCC structure, *i.e.* we neglect a small tetragonal distortion in ice VIII. The BCC structure is made of two interpenetrating FCC (Ic) sublattices. Only 6-membered rings, *i.e.* the shortest closed loops of connected bonds, are contained in the 16-molecule simulation cell. There is one such ring per FCC sublattice. As elsewhere in this work, we adopt the three-state model discussed above. The convention presently used is that the near side is located clockwise to the left side of the bond. In ice VIII, the anti-ferroelectric arrangement of the two proton ordered sub lattices yields proton patterns with three consecutive N and three consecutive F states that are anti-correlated with respect to each other in the two rings. In ice VII, quantum fluctuations disorder the patterns but in the simulation there is still residual anti-correlation among the two sublattices. This result is due to the finite size of the cell and is in agreement with the findings of Ref. [15]. The probability of a ring configuration possessing a consecutive block of N, F, or C states is given in Fig. 6. This is contrasted to the distribution one would attain if the proton states along the bonds were randomly distributed with probabilities $P_N = P_F = 2P_C$, as predicted by a mean field model. We find that longer "blocks" are favored in the simulation in contrast to the random case. Notice that the very small size of the simulation cell prevents us from studying quantitatively the spatial extent of proton correlations, but Fig. 6 suggests that concerted jumps on rings longer than 6-fold should be present in the real crystal. At the same time the figure shows that the number of configurations that correspond

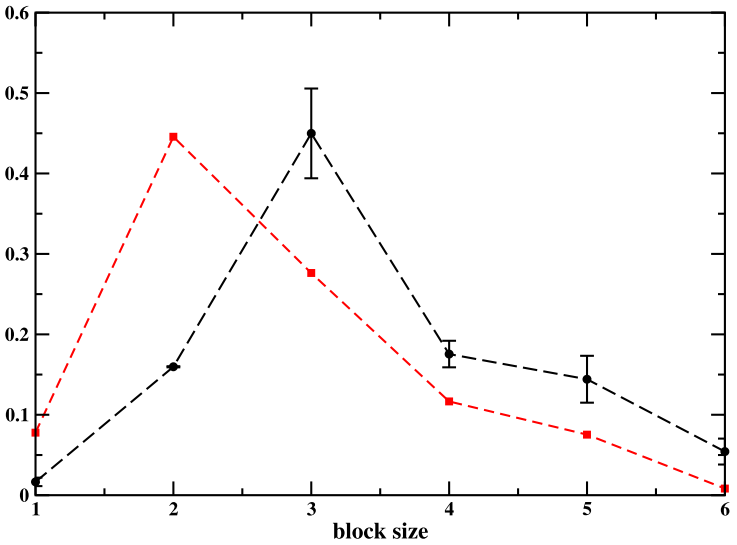

Fig. 6 (Color online) The probability of a ring configuration having a consecutive block of N, F, or C states of length L (*black dashed line* with circles and error bars). The *red dashed line* with squares is the resultant random distribution where the probability of drawing an N or F on a bond along the ring is twice that of drawing a C

to concerted ring tunneling *i.e*. *NNNNNN*, *FFFFFF*, or *CCCCCC* comprise less than 10% of configurations. This finding indicates that mechanisms which violate local charge neutrality do occur, albeit to a much smaller degree than in the mean field model and compete with concerted tunneling processes for state changes.

5 Effective Proton Potential

The environmental changes occurring in the H bond symmetrization process are well illustrated by introducing the effective potential that, in the 1D Schrödinger equation for the proton dynamics along the bond, gives a ground state solution that simultaneously fits the position and end-to-end distributions. This is possible in ice Ih and VIII as these systems are ground state dominated.

Both ice Ih and VIII exhibit "typical" hydrogen bonding and we utilize the following functional form for the effective potential:

$$V(x) = a_3(x - x_0)^3 + a_2(x - x_0)^2. \tag{12}$$

The parameters for the fits are given in Table 3. The corresponding potentials are given in Fig. 7 and the resulting position and end-to-end distributions are compared with the raw data in Fig. 8.

In ice Ih and VIII the proton is localized in a covalent well and the model potential includes harmonic confinement and an anharmonic cubic correction. One may notice that in ice VIII (see Table 1) the spatial distribution is narrower near the maximum and at the same time spills out more towards the distant O. Overall, however, the proton is more confined in

Table 3 Parameters for the cubic potential in (12) for ice Ih and ice VIII. a_n is given in meV/Å^n and x_0 is given in Å

Phase	a_2	a_3	x_0
Ih	15450	−30666	0.011
VIII	19143	−49764	0.016

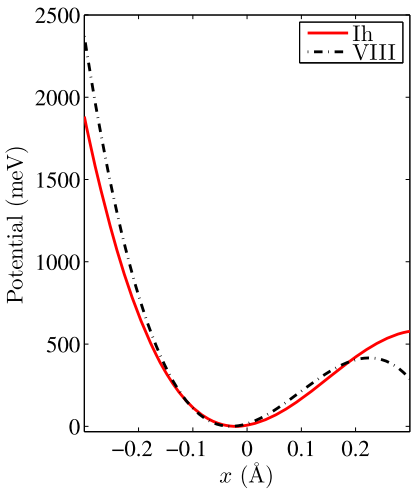

Fig. 7 (Color online) The effective cubic potential for ice Ih (*red solid line*) and ice VIII (*black dashed line*) along hydrogen bond direction

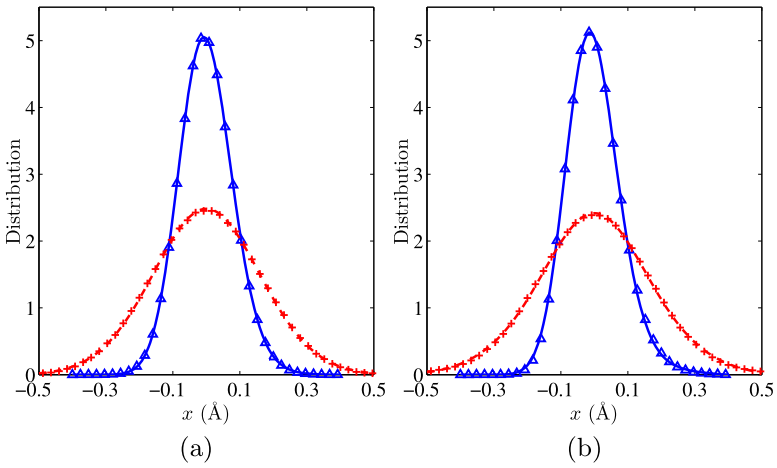

Fig. 8 (Color online) (**a**) The position distribution of ice Ih obtained from the PICPMD simulation (*blue solid line*) and that reconstructed from the cubic potential (*blue triangle*), together with the end-to-end distribution of ice Ih obtained from the PICPMD simulation (*red dashed line*) and that reconstructed from the cubic potential (*red cross*); (**b**) The position and the end-to-end distributions in ice VIII. The legend is the same as in (**a**)

ice VIII than in ice Ih. The potential in Fig. 7 reflects this behavior and shows clearly greater anharmonicity (and skewness) in ice VIII than in ice Ih.

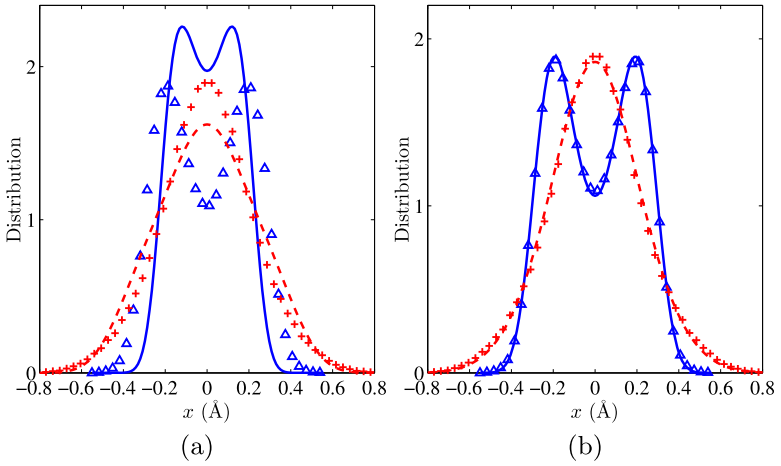

Fig. 9 (Color online) (**a**) The position distribution of ice VII obtained from the PICPMD simulation (*blue solid line*) and that reconstructed from a double well potential (*blue triangle*), together with the end-to-end distribution of ice VII obtained from the PICPMD simulation (*red dashed line*) and that reconstructed from the same double well potential (*red cross*). A unique potential cannot accurately fit the position and end-to-end distributions of ice VII. (**b**) The position distribution of ice VII obtained from the PICPMD simulation (*blue solid line*) and that reconstructed from a three-state potential ensemble (*blue triangle*), together with the end-to-end distribution of ice VII obtained from the PICPMD simulation (*red dashed line*) and that reconstructed from the same three-state potential ensemble (*red cross*)

Interestingly, in ice VII no unique potential that simultaneously fits the position and end-to-end distributions can be found, even though the system remains ground state dominated. As explained in Sects. 3 and 4 this is because the proton is in an entangled state reflecting short range correlations with the other protons that originate from the requirement of local charge neutrality. The tunneling proton is well described in terms of a three-state model corresponding to three distinct positions of the centroid of the Feynman path along the bond: N, C, and F (see Sect. 4). This suggest that position and end-to-end distributions should be fitted using a mixed ensemble in which three distinct potentials are used to model the 3 states of the proton. For the three potentials we adopt the following form:

$$\begin{aligned} V_N(x) &= a_4x^4 + a_2x^2 + a_1x, \\ V_C(x) &= a_4x^4 + a_2x^2, \\ V_F(x) &= a_4x^4 + a_2x^2 - a_1x. \end{aligned} \tag{13}$$

Each potential i generates a position and end-to-end distribution, respectively. The total position and end-to-end distributions are given by the ensemble average

$$\begin{aligned} n(x) &= \omega_N n_N(x) + \omega_C n_C(x) + \omega_F n_F(r), \\ \widetilde{n}(x) &= \omega_N \widetilde{n}_N(x) + \omega_C \widetilde{n}_C(x) + \omega_F \widetilde{n}_F(x), \end{aligned} \tag{14}$$

with weights given by $\omega_F = \mu, \omega_C = 1 - 2\mu, \omega_F = \mu$, respectively. Using a, b, c, μ as optimization parameters, both position and end-to-end distributions can be accurately reproduced as shown in Fig. 9(b). The three types of potentials are depicted in Fig. 10. It is found that both the position and the end-to-end distributions are fitted accurately with

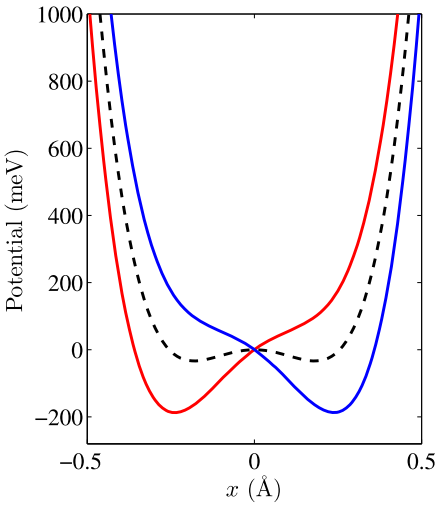

Fig. 10 (Color online) Three-state potential ensemble for ice VII. The two tilted potentials (*blue and red lines*) have equal weights $\omega_N = \omega_F = 0.40$, the double well potential (*dashed black line*) has weight $\omega_C = 0.20$

Table 4 Parameters for the three-state potential ensemble for ice VII and ice X. a_n is given in meV/Å^n

Phase	a_1	a_2	a_4
VII	725	−2038	31511
X	1645	−1263	8922

$\omega_N = \omega_F = 0.40$ and $\omega_C = 0.20$, which is consistent with the analysis in Sect. 4. Notice, however, that the three corresponding states of the proton overlap and are not orthogonal: thus the three weights $\omega_N, \omega_C, \omega_F$ are not equivalent to the eigenvalues of the density matrix discussed in Sect. 3. V_N, V_F are tilted towards one or the other side of the hydrogen bond by the linear term in (13). This term has the effect of lowering the potential when the proton is on the bond side that maintains charge neutrality at the nearest oxygen site. Thus V_N, V_F break inversion symmetry relative to the bond center penalizing ionized configurations. V_C is a double well potential, with the potential barrier lower than the zero-point motion energy.

It should be noted that a two-state model for the proton and the corresponding two-state potential ensemble is sufficient to capture the main qualitative features of the position and end-to-end distributions, but the fit is less accurate than the one provided by the adopted three-state model. There are physical reasons for this finding. Fractional charge fluctuations are allowed in the 3-state model while only integer charge fluctuations are possible within the 2-state model. Fractional charge fluctuations minimize the deviation from local charge neutrality (see Sect. 4). Moreover the 3-state model mimics an effect of the coupling of the proton with the lattice: when the proton is in C the bond length is on average slightly shorter than when it is in N or F. A similar correlation was already reported in Ref. [15]: it indicates that quantum fluctuations couple with the geometrical structure, an effect that is quite important in KDP where it leads to the so-called Ubbelohde effect upon isotopic substitution [29].

Mixed state character is not as prominent but still noticeable in our ice X sample. In this case the best fit is provided by the same potential ensemble (13) with the parameters given in the second row of Table 4. We find that position and the end-to-end distributions are fitted accurately with $\omega_N = \omega_F = 0.05$ and $\omega_C = 0.90$, as illustrated in Fig. 11. The proton in ice X is predominately in the C state, consistent with the LBHB character.

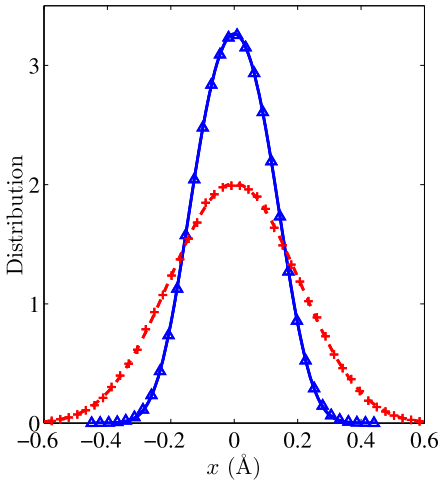

Fig. 11 (Color online) The position distribution of ice X obtained from the PICPMD simulation (*blue solid line*) and that reconstructed from a three-state potential ensemble (*blue triangle*), together with the end-to-end distribution of ice VII obtained from the PICPMD simulation (*red dashed line*) and that reconstructed from the same three-state potential ensemble (*red cross*)

6 Conclusion

In this work we have quantified the role played by correlations in the proton disordering transition occurring when antiferroelectric ice VIII converts to paraelectric ice VII. At sufficiently low temperature this transition is driven mostly by quantum fluctuations that lead to tunneling and delocalization of the protons in the bonds that connect the oxygen vertices in the crystalline lattice. To analyze the PICPMD simulation data we used two concepts that are new in this context. We performed a spectral decomposition of the single particle density matrix, a property that is available in simulations that sample not only the spatial distribution of the quantum particles but also their momentum distribution, or equivalently the end-to-end distribution of the open Feynman paths. The spectral analysis of the density matrix allowed us to assess unambiguously the role of correlations by quantifying the entanglement of the proton state, its deviation from the prediction of mean field theory, and the characteristic energy scale of the entanglement, which turned out to be much larger than $k_B T$. Next, we monitored the centroids of the paths to study, in particular, concerted ring fluctuations of the centroids. This analysis allowed us to associate unambiguously proton correlations to local charge neutrality. The latter requirement generalizes the so-called ice rule due to Bernal, Fowler and Pauling [10, 11], which applies to coarse grained models with two proton sites on each bond. Local charge neutrality is basically a classical concept, and it is an interesting observation that this simple classical construct drives subtle quantum correlations in ice VII.

The standard picture used to interpret previous PICPMD studies of the H bond symmetrization transitions at high pressure was based on mean field theory and did not take into account the correlations present in the simulations. This picture is illustrated in Fig. 1: it assumes that in ice VII each proton tunnels coherently back and forth between two sites (N and F) on the opposite sides of a bond. This process, if random, would lead to a large number of ionized configurations, such as H_3O^+ and OH^- or H_4O^{++} and O^{--}, but this so-called ionization catastrophe [12] is penalized by the energy cost of dissociating the water molecules. To avoid this cost, concerted tunneling processes take place that reduce the number of ionized configurations. However, charged defects are not entirely suppressed as if only complete ring tunneling jumps were allowed. Because of correlations the state of the proton that at low enough temperature is essentially a pure quantum state in ice VIII,

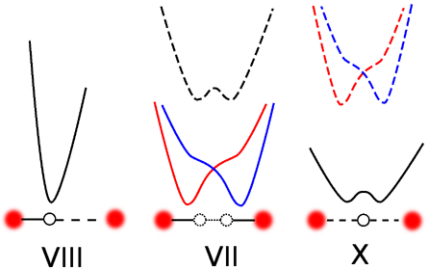

Fig. 12 (Color online) Classification of H bonds established in this paper: The proton in ice VIII (and in ice Ih) is in a pure quantum state and experiences an asymmetric single well potential that keeps it localized on one side of the bond. The proton in ice VII (HBHB) and in ice X (LBHB) is in a mixed quantum state and experiences a potential ensemble that depends on its location on the bond. Dominant potentials are indicated by *full lines* and less dominant ones by *dashed lines*. The proton distribution is symmetric and bimodal in ice VII and symmetric and unimodal in ice X

becomes a mixed quantum state in ice VII and to some extent as well in ice X, where charge fluctuations on the bonds are present and the system is in the so-called LBHB regime. The mixed state character can be described in terms of a potential ensemble, as illustrated in Fig. 12. The new picture provides a more accurate description of the H bond symmetrization transitions than Fig. 1.

Several questions remain open, such as whether or not concerted tunneling processes occur on rings longer than 6-fold with measurable frequency or how do collective fluctuations decay in space. Some answers to these questions may come from future simulations on larger cells. For instance, simulations on cells that are at least 8 times bigger than the present 16 molecule one would be feasible on modern supercomputers. These simulations could take advantage of algorithms like a newly proposed estimator of the end-to-end distribution [30] to improve accuracy and statistics. Other issues involve the entropy change between the ordered and the disordered phase. Overall it is important to understand the precise nature of the quantum many-body ground-state of the protons in the disordered phase and the nature of the corresponding excitation spectrum. Coarse grained models using a spin Hamiltonian to describe the proton system may be very useful in this respect and could benefit from input from realistic off-lattice simulations like the present one. For instance, the present simulation suggests that a spin 1 model should provide a more accurate representation of the protons in ice VII than a spin $1/2$ model.

Finally, the present study has implications for other H-bonded systems where proton tunneling occurs. Ring tunneling processes like those that we have observed here have been hypothesized to occur on ordered rings in ice Ih at low temperature to explain isotope effects in the quasi-elastic neutron peak [31]. In ice Ih the bond length is significantly longer than in ice VII and concerted tunneling should have a much lower frequency than in the present simulation. However, the system for which the present results has more direct implications is KDP, an H-bonded molecular crystal which is ferroelectric at very low temperature and undergoes a transition to a paraelectric phase driven by quantum fluctuations at $T_c = 121$ K. The phosphate groups in KDP are in a local tetrahedral environment and are linked together by H bonds as the water molecules in ice. The ferro-to-para transition corresponds to disordering of the H sublattice. The processes that we find in each ferroelectrically ordered sublattice of ice VIII upon transition to ice VII at low temperature should have strong similarities with the quantum fluctuations that lead to the disordering transition in KDP.

Acknowledgements This research was supported by the NSF under grand CHE-0956500 and by the DOE under grant DE-SC0005180. J.M. acknowledges the Fannie and John Hertz Foundation.

Appendix: Test of Independence Using Spearman's Rank Correlation Coefficient

In this appendix we give a short introduction to the test of independence using Spearman's rank correlation coefficient and apply it to illustrate the separation of the potential energy surface along and perpendicular to the hydrogen bonding direction for ice Ih, VIII, VII and X.

Consider a series of observation points $(X_i, Y_i)_{i=1}^N$ coming from a two dimensional continuous random variable (X, Y). In this case X is the end-to-end distance along the hydrogen bonding direction and Y is the end-to-end vector projected on the plane orthogonal to the hydrogen bonding direction. If X and Y are independent, the effective potential experienced by the proton should separate along the hydrogen bonding direction and the orthogonal direction. We sort $\{X_i\}_{i=1}^N$ in ascending order as $X_{S_1}, \ldots, X_{S_N}$, and S_i is called the rank of X_i. Similarly we define T_i to be the rank of Y_i. Spearman's rank correlation coefficient is defined to be the correlation between the pairs $(S_i, T_i)_{i=1}^N$ *i.e.*

$$R = \frac{\sum_{i=1}^N (S_i - \bar{S})(T_i - \bar{T})}{\sqrt{\sum_{i=1}^N (S_i - \bar{S})^2 \sum_{i=1}^N (T_i - \bar{T})^2}}, \tag{15}$$

with

$$\bar{S} = \bar{T} = \frac{N+1}{2}. \tag{16}$$

Spearman's rank correlation coefficient can be expressed in the more convenient form as

$$R = \frac{12}{N(N+1)(N-1)} \sum_{i=1}^N S_i T_i - 3\frac{N+1}{N-1}. \tag{17}$$

The advantage of Spearman's rank correlation coefficient is that it is based on the rank of X and Y rather than on the detailed behavior of these random variables. As a result, Spearman's rank correlation coefficient can be used as a test of independence without assuming that (X, Y) follows a Gaussian distribution. This is particularly useful in the present context because we know that anharmonicity exists at least along the hydrogen bonding direction, and the end-to-end distribution along the hydrogen bonding direction is not Gaussian. Furthermore, $R = \pm 1$ occurs only if X and Y are functionally dependent on each other. This dependence can be linear or non-linear. If Spearman's rank correlation coefficient is 0 then X and Y are independent.

References

1. Andreani, C., Colognesi, D., Mayers, J., Reiter, G., Senesi, R.: Adv. Phys. **54**, 377 (2005)
2. Soper, A., Benmore, C.: Phys. Rev. Lett. **101**, 65502 (2008)
3. Morrone, J.A., Car, R.: Phys. Rev. Lett. **101**, 017801 (2008)
4. Bratos, S., Diraison, M., Tarjus, G., Leicknam, J.C.: Phys. Rev. A **45**, 5556 (1992)
5. Ramirez, R., Lopez-Ciudad, T., P, P.K., Marx, D.: J. Chem. Phys. **121**, 3973 (2004)
6. Paesani, F., Iuchi, S., Voth, G.A.: J. Chem. Phys. **127**, 074506 (2007)

7. Habershon, S., Fanourgakis, G.S., Manolopoulos, D.E.: J. Chem. Phys. **129**, 074501 (2008)
8. Beck, T.L.: Free Energy Calculations: Theory and Applications in Chemistry and Biology. Springer, Berlin (2007) (Chap. 11, p. 387)
9. Lin, L., Morrone, J.A., Car, R., Parrinello, M.: Phys. Rev. B **83**, 220302(R) (2011)
10. Bernal, J., Fowler, R.: J. Chem. Phys. **1**, 515 (1933)
11. Pauling, L.: J. Am. Chem. Soc. **57**, 2680 (1935)
12. Stillinger, F., Schweizer, K.: J. Phys. Chem. **87**, 4281 (1983)
13. Schweizer, K., Stillinger, F.: Phys. Rev. B **29**, 350 (1984)
14. Schweizer, K., Stillinger, F.: J. Chem. Phys. **80**, 1230 (1984)
15. Benoit, M., Marx, D., Parrinello, M.: Nature **392**, 258 (1998)
16. Morrone, J.A., Lin, L., Car, R.: J. Chem. Phys. **130**, 204511 (2009)
17. Neto, A., Pujol, P., Fradkin, E.: Phys. Rev. B **74**, 024302 (2006)
18. Bramwell, S., Gingras, M.: Science **294**, 1495 (2001)
19. Feynman, R., Hibbs, A.: Quantum Mechanics and Path Integrals. McGraw-Hill, New York (1965)
20. Chandler, D., Wolynes, P.: J. Chem. Phys. **74**, 4078 (1981)
21. Hohenberg, P., Kohn, W.: Phys. Rev. **136**, B864 (1964)
22. Kohn, W., Sham, L.: Phys. Rev. **140**, A1133 (1965)
23. Car, R., Parrinello, M.: Phys. Rev. Lett. **55**, 2471 (1985)
24. Marx, D., Parrinello, M.: J. Chem. Phys. **104**, 4077 (1996)
25. Tuckerman, M., Marx, D., Klein, M., Parrinello, M.: J. Chem. Phys. **104**, 5579 (1996)
26. Marx, D., Tuckerman, M., Martyna, G.: Comput. Phys. Commun. **118**, 166 (1999)
27. Morrone, J.A., Srinivasan, V., Sebastiani, D., Car, R.: J. Chem. Phys. **126**, 234504 (2007)
28. Benoit, M., Marx, D.: Chem. Phys. Chem. **6**, 1738 (2005)
29. Robertson, J., Ubbelohde, A.: Proc. R. Soc. Lond. Ser. A **170**, 222 (1939)
30. Lin, L., Morrone, J.A., Car, R., Parrinello, M.: Phys. Rev. Lett. **105**, 110602 (2010)
31. Bove, L.E., Klotz, S., Paciaroni, A., Sacchetti, F.: Phys. Rev. Lett. **103**, 165901 (2009)